Pergamon

J. Geodynamics Vol. 26, No. 2–4, pp. 353–365, 1998

PII: S0264-3707(97)00079-3
0264-3707/98 $19.00+0.00

CRUSTAL AND UPPER MANTLE STRUCTURE OF THE KOZANI–GREVENA AREA OBTAINED BY NON-LINEAR INVERSION OF P AND S TRAVEL TIMES

C. B. PAPAZACHOS,[1] V. G. KARAKOSTAS[2] and E. M. SCORDILIS[2]

[1]Institute of Engineering Seismology and Earthquake Engineering, PO Box 53, Foinikas, GR-55102 Thessaloniki, Greece
[2]Geophysical Laboratory, University of Thessaloniki, PO Box 352-1, GR-54006 Thessaloniki, Greece

(Received 8 January 1997; revised 12 August 1997; accepted 14 August 1997)

Abstract—The present study focuses on the P and S crustal and uppermost mantle velocity structure in the broader Kozani–Grevena area. The velocity structure is derived from the inversion of travel times of local events. The main data source is the travel times from the aftershock sequence of the large event of 13 of May 1995 ($M_w = 6.6$) which occurred in the study area. An appropriate preconditioning of the final linearized system is used to reduce ray density effects on the results. An attempt is made to interpret the features and details of the crustal structure in terms of the geotectonic setting of the area. The observed features of the deeper crustal and uppermost mantle structure are in very good agreement with previous results. Specifically, a crustal thickening is observed along a ENE–WSW direction, perpendicular to the well-known Dinaric trend (NNW–SSE) of the geological formations of the area, in accordance with the theoretical expectation of a thicker crust under the accretion prism which starts at the SW edge of the study area.

INTRODUCTION

The Aegean sea (Fig. 1) is one of the seismically most active regions worldwide. In the southern part of the area, the main feature is the subduction of the eastern Mediterranean lithosphere under the Aegean (Papazachos and Comninakis, 1969; McKenzie, 1970, 1978; LePichon and Angelier, 1979). The tectonic pattern of the area is fairly typical for a subduction system with shallow events, thrust in the outer arc and normal in the back-arc area (Comninakis, 1975; McKenzie, 1978). On the other hand, a shallow dipping Benioff zone is delineated by the intermediate depth seismicity (Papazachos and Comninakis, 1969, 1971) and a well defined volcanic arc is formed by a number of volcanoes, which coincides with the 150 km isodepth of this Benioff zone. This complicating geotectonic setting as well as the complex evolution of the area has left a strong signature on the geological environment of the area which is reflected in the velocity structure. Refraction experiments (Makris, 1976), travel time studies (Panagiotopoulos and Papazachos, 1985; Papazachos and Nolet,

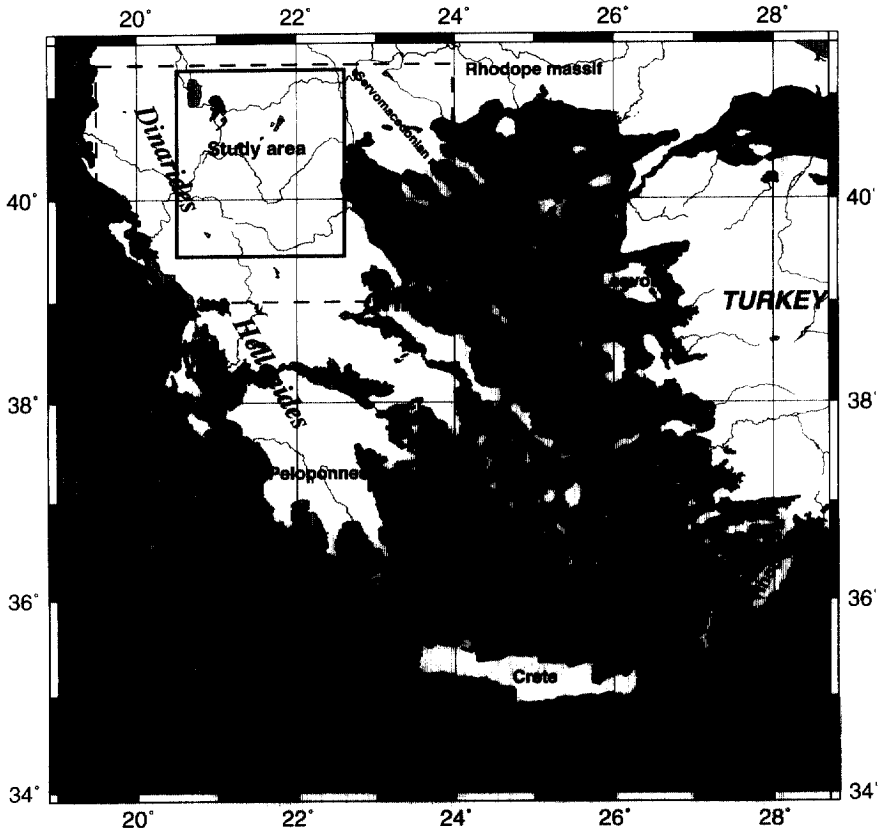

Fig. 1. General features of the Aegean area. The study area is delineated by a solid line, while the dashed line bounds the area covered by the recording stations.

1997a) and gravity modeling (Makris, 1973; Chailas *et al.*, 1992; Papazachos, 1994) show significant variations throughout the whole Aegean lithosphere. The main crustal variations can be explained within the context of the active subduction: The Hellenic Alps (Hellenides) which also represent the Hellenic Arc accretionary prism (Fig. 1) show a crustal thickening which locally reaches 45 km. On the other hand, the back-arc area exhibits a much thinner crust of the order of 25–30 km.

The broader Kozani–Grevena area lies in the western part of northern Greece. The area is dominated by the Pindos mountains which is the main body of the Hellenic Alps. The main geologic formations are the Mesozoic metamorphic and calcacitic formations of the Pelagonian and Vardar geologic zones which are overlayed by the molassic formations of the Kozani–Grevena basin (Mountrakis, 1985). In this area, the Hellenides follow the well-known Dinaric trend (NNW–SSE) and represent the accretion prism of the present subduction of the Eastern Mediterranean lithosphere beneath the Aegean area. Large scale tomographic studies (Papazachos and Nolet, 1997a) show that the crustal variations follow the general pattern: a gradual thickening is observed as we move from the ENE to WSW, that is perpendicular to the Dinaric trend.

In the present paper, the detailed characteristics of the velocity structure of the broader NW Greece is studied, with an emphasis in the Kozani–Grevena area. This area has been extensively studied (e.g. Papazachos *et al.*, 1996; Hatzfeld *et al.*, 1997), after the large destructive event of the 13th of May 1995 ($M_w = 6.6$, h = 14 km, 40.15°N, 21.68°E). This event was the largest in the study area during the present century and resulted in significant damage in the area, also due to its large aftershock sequence: more than a thousand earthquakes were recorded by the local and regional network and more than 100 of them had $M_w > 4.0$. The main modification to the standard tomographic approach is the use of a modified inversion technique (Papazachos and Nolet, 1997b) which incorporates 3-D ray tracing. S waves are also included in the present study. We mainly focus in the structure of the shallow crust and its association with the broader area of the large Kozani earthquake. Moreover, we study the deeper crustal and uppermost mantle structure of the broader area and its correlation with the major geotectonic features of the Aegean area.

TRAVEL TIME DATA

The study area is delineated with the thick solid line in Fig. 1. The main source of travel-time data is the annual and monthly bulletins of the Geophysical Laboratory of the University of Thessaloniki (GLUT) for the time period 1981–1995. A large part of the data set came from the monthly bulletins of seismological observatories of Greece and neighboring countries. Moreover, we included data collected from a local seismicity monitoring network operated in the area between the 19 and the 26 of May 1995, which was installed to monitor the post-seismic activity of the large destructive event of 13 of May, 1995 (Hatzfeld *et al.*, 1997). Finally, travel times from the network operated by the Public Electric Power Company were also included in the data set. The area covered by the recording stations is depicted by a thick dashed line in Fig. 1. All events are initially relocated by the GLUT using an appropriate model for the Greek area (Panagiotopoulos and Papazachos, 1985), except for the events recorded by the local network which were located by a modified local model (Hatzfeld *et al.*, 1997). During this relocation process travel times were checked for outliers and other sources of errors, resulting in a high quality data set.

A typical problem in local studies is the 'contamination' of the results due to the presence of mislocated earthquakes. Therefore, certain criteria were established for the data selection based on the results of a previous analysis of earthquake locations for Greece (Karakostas, 1988). Hence, only events with at least 8 P and 1 S phases were used. Moreover, phases reported as impulsive were assigned a higher weight (typically a factor of 2). Also, the accuracy of the data used in present study varies considerably, as revealed by the relocation process. Stations of the post-seismic monitoring network show much smaller errors (typically 0.1 sec) than analog recordings in the area (typically 0.2 sec for P and 0.5 sec for S) or digital recordings from the regional network (typically 0.7–1.0 sec). All these estimations were taken into account and relative phase weights were assigned. The final data set consists of 47793 P and 30006 S arrivals, from more than 3700 events recorded at 43 permanent and 39 temporary stations. The final epicenters of the events for which data were used and the station locations are depicted in Fig. 2, where the study area is delineated by a thick solid line.

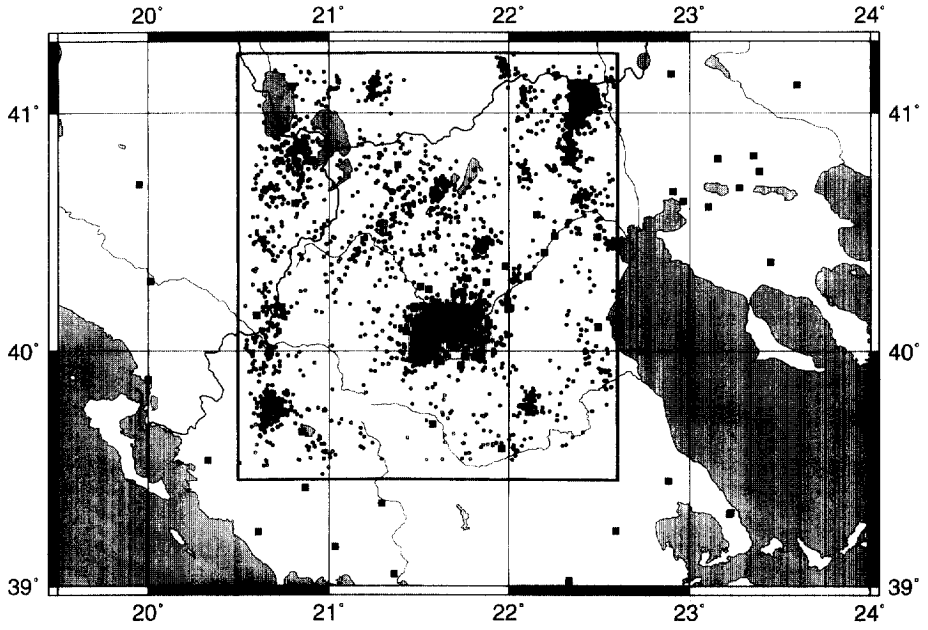

Fig. 2. Map of the epicenters (denoted with circles) of the events for which data were used in the present study. Permanent and temporary stations are depicted by solid squares.

TRAVEL TIME INVERSION

The aim of the travel-time inversion of local earthquakes is to simultaneously determine the velocity structure and relocate the earthquakes in the new 3-D velocity medium, as in the pioneering work of Aki and Lee (1976). The travel time residual is expressed as a function of the perturbations of the event's hypocentral parameters and the slowness model, which is linearized using initial approximate parameters (e.g. derived from 1-D ray theory). A linear system of equations is derived:

$$\mathbf{d} = \mathbf{Bh} + \mathbf{Cv} + \mathbf{c} \tag{1}$$

where **d** contains the travel time residuals, **B** and **C** are the hypocentral and velocity derivative matrices, **h** and **v** are the hypocentral and velocity corrections vectors and **c** is a station correction vector which is included to account for anything that can not be explained by the retrieved velocity structure (e.g. velocity structure beneath a station or outside the area for which velocities are determined, etc.). Clearly, Eq. (1) can be rewritten as a simple linear system of the form:

$$\mathbf{d} = \begin{bmatrix} B & 0 & 0 \\ 0 & C & 0 \\ 0 & 0 & I \end{bmatrix} \begin{bmatrix} h \\ v \\ c \end{bmatrix} = Ax \tag{2}$$

where

$$\mathbf{A} = \begin{bmatrix} B & 0 & 0 \\ 0 & C & 0 \\ 0 & 0 & I \end{bmatrix}$$

I is the identity matrix and

$$\mathbf{x} = \begin{bmatrix} h \\ v \\ c \end{bmatrix}.$$

Therefore, **A** contains all the velocity and hypocentral derivatives for each travel-time and **x** contains all the necessary hypocentral and velocity corrections that should be applied to our initial model (velocity and event parameters), as well as appropriate station corrections.

In the present study a trilinear interpolation function was chosen for the model representation (Thurber, 1983). The usual problem with tomographic studies is that the model is not properly sampled by the available seismic rays. Therefore, the inversion problem is partly underdetermined and the linear system of Eq. (2) does not have a unique solution. Usually, an appropriate solution is constructed by considering additional constraints and minimizing e.g. the model or the model second derivative norms (Franklin, 1970; Tarantola and Nercessian, 1984; Constable *et al.*, 1987). In the present study Eq. (2) is modified (Papazachos and Nolet, 1997a), as follows:

$$\begin{aligned} \mathbf{C}_d^{-1/2}\mathbf{A}\mathbf{C}_x^{1/2}\mathbf{S}\mathbf{H}\mathbf{z} &= \mathbf{C}_d^{-1/2}\mathbf{d} \\ \lambda\mathbf{I}\mathbf{z} &= \mathbf{0} \end{aligned} \tag{3}$$

were $\mathbf{C}_d$ is the data covariance matrix, $\mathbf{C}_x$ is the *a priori* estimate of the model covariance matrix (usually diagonal), **S** is an appropriate smoothing matrix (e.g. Spakman and Nolet, 1988) and λ is a constant which regulates the strength of our additional minimum norm (damping) constraints. The inclusion of the $\mathbf{C}_x$ matrix in Eq. (3) ensures that all parameters (velocity and event perturbations as well as station corrections) are scaled to their *a priori* errors so that vector **d** is non-dimensional and all parameters are treated in the same manner when solving Eq. (3). Matrix **S** is included in Eq. (3) so that the constructed solution is chosen to be smooth (depending on the structure of matrix **S**). Here, an additional diagonal scaling matrix of the form $\mathbf{H} = \mathrm{diag}\{\mathrm{h}_j^{-1/2}\}$ is included, where h_j is a measure of the j*th* column length of the matrix $\mathbf{A}' = \mathbf{C}_d^{-1/2}AC_x^{1/2}$ S. In this approach, $\mathbf{x}^T C_x^P x$ is minimized, instead of the usual $\mathbf{x}^T\mathbf{C}_x\mathbf{x}$, where bold $(C_x^P)^{1/2} = C_x^{1/2}\mathbf{SH}$ is our preliminary estimate of the square root of the *a posteriori* model covariance matrix, in an attempt to reduce relative errors in the final solution (Papazachos and Nolet, 1997a)

For the present study, the velocity grid consisted of 14256 P and S velocity nodes with a horizontal and vertical grid spacing of 15 km and 3 km, respectively. The initial velocity values were determined after a simple 1-D inversion. A cut-off residual of 2.5 s for the recordings of the regional stations was adopted from previous studies (e.g Karakostas, 1988) to eliminate the effect of outliers. For the recordings of the temporary Kozani network these limits were reduced to 0.4 s for P and 0.7 s for S arrivals, as indicated by the 1-D relocations. Moreover, appropriate values were determined for the variance of the P and S slowness perturbation norms as well as for the hypocentral station corrections, from previous results (e.g. Scordilis, 1985; Karakostas, 1988; Papazachos and Nolet, 1997a).

Equation (3) was solved with LSQR (Paige and Saunders, 1982) which has superior

converging and stability properties. After each LSQR iteration **A** was recomputed using a revised 3-D bending ray tracing algorithm (Moser *et al.*, 1992) and the new linear system was repeatedly solved until no significant misfit change was observed. Between successive iterations a misfit increase was observed, due to the non-linearity of the problem: As rays are retraced in the new velocity model the real non-linear misfit is computed (after each iteration) which is larger than the linearized misfit which is minimized by LSQR in the previous iteration. This observation is in accordance with recent tomographic studies and synthetic tests (Sambridge, 1990; Papazachos and Nolet, 1997b). As we converge to the final model, the rays are practically not modified between iterations, hence this misfit increase is almost insignificant.

The final residual distribution for P and S arrivals before and after the inversion is shown in Fig. 3. One can notice that the residual distribution before the inversion shows a significant skewness. This is probably due to two different reasons. The first reason is the strong 3-dimensional structure of the area. Since all events are initially relocated using a 1-dimensional velocity model, the travel-time residuals do not necessarily follow a normal distribution. This is caused because the presence of strong 3-dimensional anomalies can

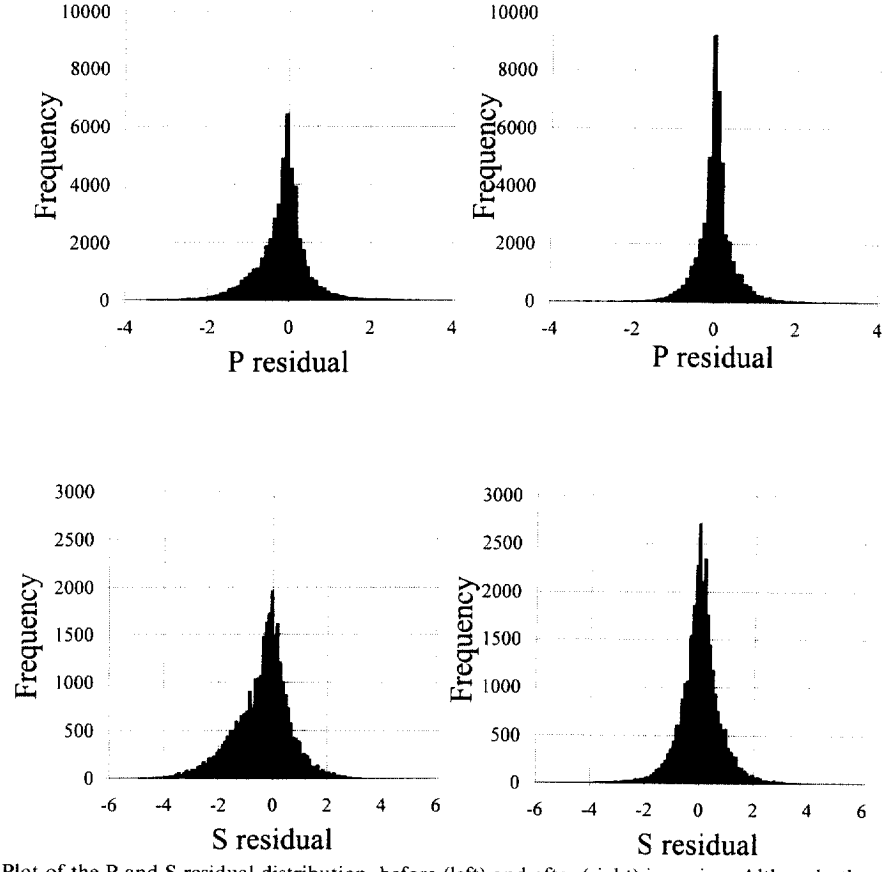

Fig. 3. Plot of the P and S residual distribution, before (left) and after (right) inversion. Although, the residuals distribution is significantly improved in the final results, it is quite different from Gaussian (long-tailed).

result in a systematic 'shifting' of the travel time residuals for certain parts of the examined area. The second reason is that the model used in the present study uses a linear interpolation between velocity nodes (constant velocity gradient) whereas all events were originally located in a 1-dimensional model where each layer had a constant velocity. Therefore, some travel times will also show a constant 'shifting' depending on their epicentral distance, which shows up as a skewness in the residual distribution before inversion. Of course, after the inversion this skewness is not observed as both error sources have been interpreted by the 3-dimensional velocity model.

TOMOGRAPHIC RESULTS — DISCUSSION

Figures 4, 5, 6 and 7 show the final P and S velocity distribution for different depths which focus at the upper crust (3–18 km) and the lower crustal-upper mantle (24–39 km) layers. In all figures, results are not shown for the areas which are poorly sampled by the data. This elimination of areas where the resolving power of the data is low is described in the following paragraph.

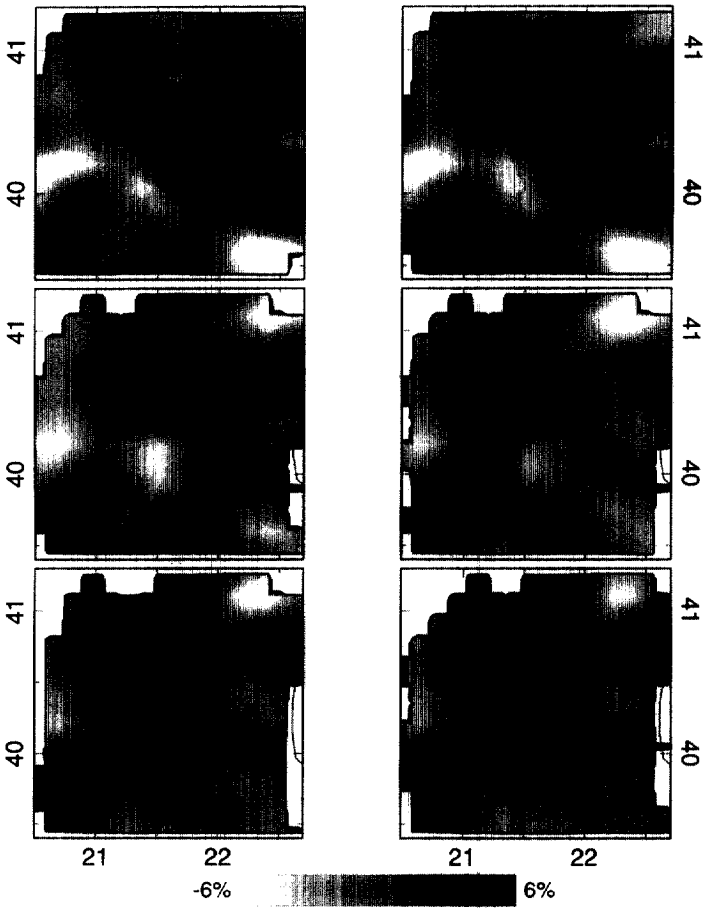

Fig. 4. P velocity perturbations for the shallow part of the final 3-D model (3–18 km).

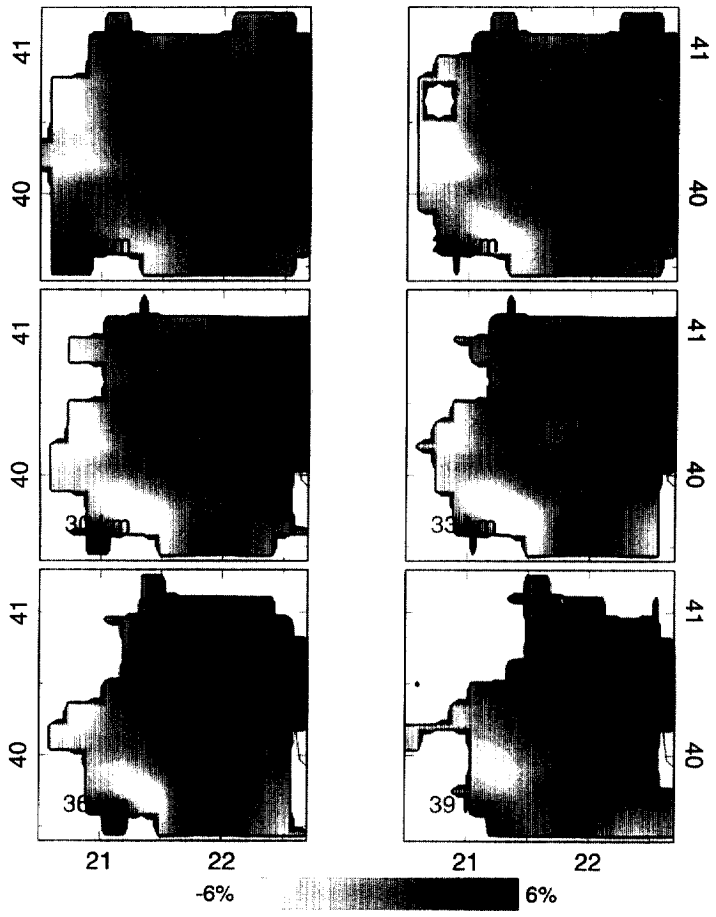

Fig. 5. P velocity perturbations for the deeper part of the final 3-D model (24–39 km).

Spike resolution tests as well as checkerboard resolution tests were performed in order to check the resolving power of the data. Using the results of these tests, a rough linear relation was established between the square root of the ray length associated with each velocity node and the relative amplitude of the recovered synthetic anomaly for the node, as this was determined from the tests. This is in agreement with the theoretical expectation that, to the first order, the relative *a posteriori* error for each velocity node is inversely proportional to the square root of the ray length associated with this node, similarly to the $1/N^{1/2}$ dependence of the expected error of a quantity which is measured N times. In all subsequent figures, we only present tomographic results for those cells where the associated ray length was large enough so that the previously determined (ray length)$^{1/2}$-(relative recovered anomaly) curve predicted a 40% for the relative recovered anomaly. Moreover, the resolution tests indicate a 5 km vertical 'leaking' for synthetic anomalies (due to the smoothing effect of matrix S in Eq. (3)) which locally reaches 10 km, in areas of poor ray coverage.

Large contrasts are observed in the shallow layers for both the P and S velocities. In

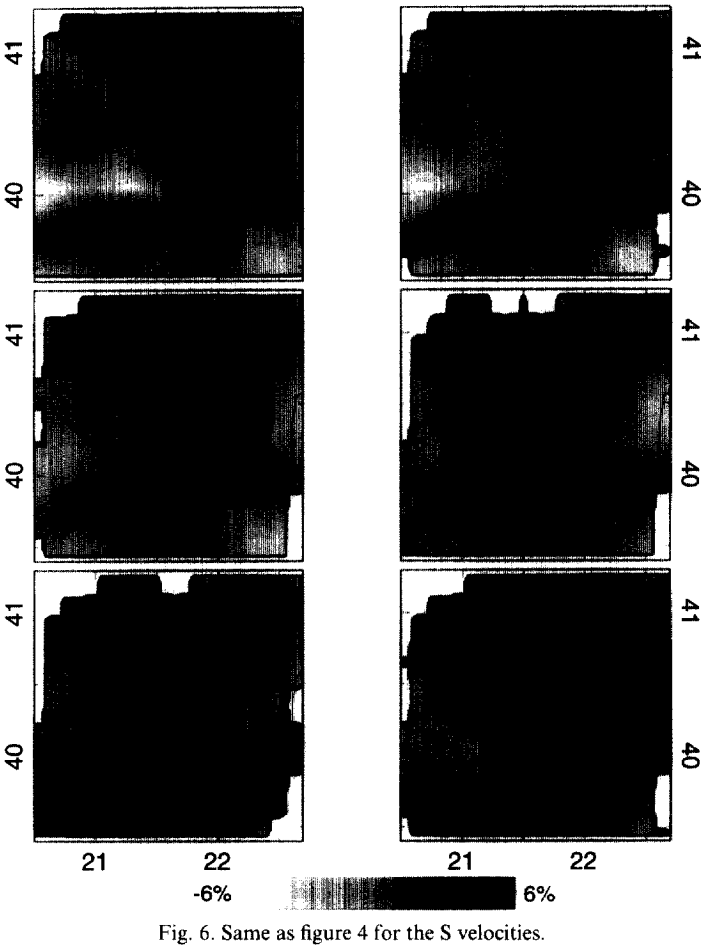

Fig. 6. Same as figure 4 for the S velocities.

the shallower layers (3–6 km), two NNW–SSE trending zones can be recognized which correspond to the two dominant geologic formations of the area. The northernmost high velocity zone corresponds to the metamorphic formations and limestones of the Pelagonian geologic belt (e.g. Mountrakis, 1985) while the southern low velocity zone corresponds to the molassic sediments of the Grevena basin. The velocity pattern becomes more complicated as we move deeper. To the northwest of this area the high velocity ophiolithic Vourinos mountain is clearly delineated. This velocity anomaly associated with the ophiolithic body seems to extend all the way up to the middle crust of the region ($\sim$24 km).

For the depth range 6–15 km, where the main seismic activity of the 13 of May 1996 event is located the epicenters recorded by the local monitoring network have been superimposed. It is interesting to notice that very low velocities can be observed in the area of the post-seismic activity. On the other hand, relatively high S velocities are observed for the same area. Hence, a special situation of velocity weakening (P) and hardening (S) coexists for the fault area. This drop of the Vp/Vs ratio is in good agreement with the expected behavior of the fault zone, close to the release of seismic energy.

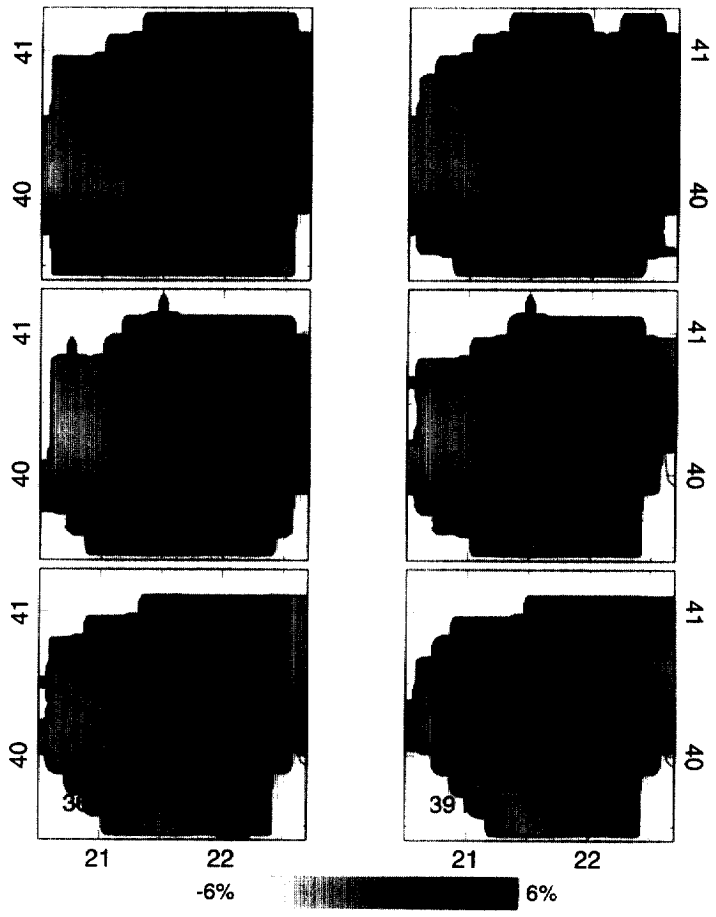

Fig. 7. Same as figure 5 for the S velocities.

The situation rapidly changes for the deeper part of the crust and the uppermost mantle (24–39 km). At these depths the velocity structure is mainly controlled by the crustal thickness variations, with high and low velocities indicating crustal thinning or thickening, respectively. A clear NNW-SSE (Dinaric) trend is observed for these depths in agreement with earlier tomographic (Papazachos *et al.*, 1995; Papazachos, 1994) and travel time (Panagiotopoulos and Papazachos, 1985) studies. Hence, a gradual Moho depth increase can be inferred as we move to the WSW edge of the study area, towards the main axis of the Hellenides mountain chain. This observation is expected from the general geotectonic setting of the Aegean area as the Hellenides represent the accretionary prism of the southern Aegean subduction system with a crust locally thickening to more than 45 km. The S velocities generally exhibit a quite good consistency with the corresponding P results, although their resolution is relatively poorer.

In Fig. 8 the P velocity distribution is plotted along two cross-sections of the area. The first profile runs perpendicular to the main axis of the fault area of the 13 of May 1996 event.

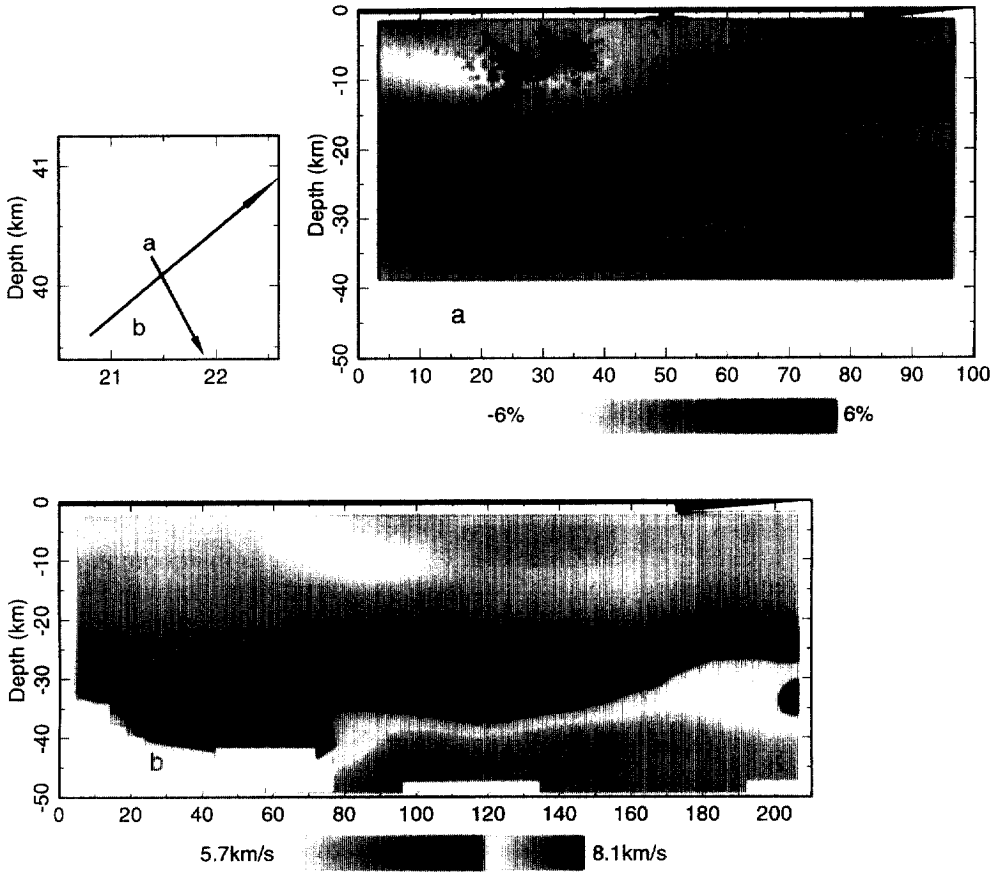

Fig. 8. P velocity distribution along the two cross-sections in the studied area. For the first cross-section (a) velocity perturbations are plotted while for the second (b) absolute velocities are shown. Notice the low velocities associated with the 13 of May 1996 ($M_w = 6.6$) event in the first cross-section and the large Moho undulation in the second (see text for explanation).

The epicenters for the 19–26 May 1996 post-seismic activity have also been superimposed on the cross-section. For this cross-section velocity perturbations are plotted instead of absolute velocities. Notice the very large P velocity drop in the area which is covered by the aftershocks sequence.

The second profile runs perpendicular to the NNW-SSE (Dinaric) trend of the area. Since in the present study only direct and transmitted (head) waves were used, it is difficult to infer accurate information about the Moho depth. Therefore, the velocity scale is separated in two areas which represent crustal and upper mantle velocities, in such a way that the Moho discontinuity is delineated. A gradual crustal thickening is observed from ~ 30 km to ~ 43 km as we move to the WSW. This crustal structure is especially interesting in connection with the geotectonic setting of the area and the general structural features of the Aegean area (e.g. Papazachos *et al.*, 1995). The maximum thickness observed is almost

equal to the maximum Moho depth under the Hellenides in the area ($\sim$45 km), as this is computed from earlier studies (e.g. Makris, 1976).

Acknowledgements—The authors would like to thank Prof. Papazachos for carefully reading the manuscript and for his fruitful suggestions. This research has partly been funded by the EEC projects ENV4-CT96-0282 and ENV4-CT96-0277.

REFERENCES

Aki, K. and Lee, W. H. K. (1976) Determination of three-dimensional velocity anomalies under a seismic array using first P arrival times from local earthquakes: 1a A homogeneous initial model. *J. Geophys. Res.* **81,** 4381–4399.

Chailas, S., Hipkin, R. G. and Lagios, E., (1992) *Isostatic studies in the Hellenides.* Proc. of the 6th Congr. of the Geological Society of Greece. 25–27 May, Athens.

Comninakis, P. E., (1975) A contribution to the investigation of the seismicity of the area of Greece. Ph.D. Thesis, University of Athens, 110pp. (in Greek).

Constable, S. C., Parker, R. L. and Constable, C. (1987) Occam's inversion: A practical algorithm for generating smooth models from electromagnetic sounding data. *Geophysics* **52,** 289–300.

Franklin, J. N. (1970) Well-posed stochastic extension of ill-posed linear problems. *J. Math. Anal. Appl.* **31,** 682–716.

Hatzfeld, D., Karakostas, V., Ziazia, M., Selvaggi, G., Leborgne, S., Berge, C., Giuguet, R., Paul, A., Voidomatis, P., Diagourtas, D., Kassaras, I., Koutsikos, I., Makropoulos, K., Azzara, R., Di Bona, M., Baccheschi, S., Bernard, P. and Papaioannou, C. (1997). The Kozani–Grevena (Greece) earthquake of May 13, 1995, revisited from a detailed seismological study. *Bull. Seism. Soc. Am.* **87,** 463–473.

Karakostas, B., (1988). Relation between the seismic activity and geological and geomorphological features of the Aegean and surrounding area. Ph.D. Thesis, University of Thessaloniki, 243pp. (in Greek).

Le Pichon, X. and Angelier, J. (1979) The Hellenic arc and trench system: a key to the neotectonic evolution of the eastern Mediterranean area. *Tectonophysics* **60,** 1–42.

Makris. J. (1973) Some geophysical aspects of the evolution of the Hellenides. *Bull. Geol. Soc. Greece* **10,** 206–213.

Makris, J. (1976) A dynamic model of the Hellenic arc deduced from geophysical data. *Tectonophysics* **36,** 339–346.

McKenzie, D. P. (1970) The plate tectonics of the Mediterranean region. *Nature* **226,** 239–243.

McKenzie, D. P. (1978) Active tectonics of the Alpine-Himalayan belt: the Aegean sea and surrounding regions. *Geophys. J. R. astr. Soc.* **55,** 217–254.

Moser, T. J., Nolet, G. and Snieder, G. (1992) Ray bending revisited. *Bull. Seism. Soc. Am.* **82,** 259–289.

Mountrakis, D.M., (1985). *Geology of Greece.* Univ. Studio Press, Thessaloniki (in Greek).

Paige, C. C. and Saunders, M. A. (1982) LSQR: An algorithm for sparse linear equations and sparse least squares. *A.C.M. Trans. Math. Softw.* **8,** 43–71.

Panagiotopoulos, D. G. and Papazachos, B. C. (1985) Travel times of Pn-waves in the Aegean and surrounding area. *Geophys. J. R. astr. Soc.* **80,** 165–176.

Papazachos, B. C. and Comninakis, P. E. (1969) Geophysical features of the Greek Islands Arc and Eastern Mediterranean Ridge. *Com. Ren. des Seances de la Conference Reunie a Madrid* **16,** 74–75.

Papazachos, B. C. and Comninakis, P. E. (1971) Geophysical and tectonic features of the Aegean arc. *J. Geophys. Res.* **76,** 8517–8533.

Papazachos, B. C., Panagiotopoulos, D. G., Scordilis, E. M., Karakaisis, G. F., Papaioannou, Ch. A., Karakostas, B. G., Papadimitriou, E. E., Kiratzi, A. A., Hatzidimitriou, P. M., Leventakis, G. N., Voidomatis, Ph. D., Peftitselis, K. I., Savaidis, A. and Tsapanos, T. M. (1996) Focal properties of the 13 May 1995 large ($M_s = 6.6$) earthquake in the Kozani area (Northern Greece). *Proc. of the XV Congress of the Carpatho–Balkan Geological Association* **6,** 96–106.

Papazachos, C. B. (1994). Structure of the crust and upper mantle in SE Europe by inversion of seismic and gravimetric data. Ph.D Thesis, University of Thessaloniki, 208 pp. (in Greek).

Papazachos, C. B. and Nolet, G. (1997a) P and S deep velocity structure of the Hellenic area obtained by robust non-linear inversion of arrival times. *J. Geophys. Res.* **102,** 8349–8367.

Papazachos, C. B. and Nolet, G. (1997b) Non-linear arrival time tomography. *Annali di Geofisica* **40,** 85–97.

Papazachos, C. B., Hatzidimitriou, P. M., Panagiotopoulos, D. G. and Tsokas, G. N. (1995) Tomography of the crust and upper mantle in southeast Europe. *J. Geophys. Res.* **100,** 12405–12422.

Sambridge, M. S. (1990) Non-linear arrival time inversion: constraining velocity anomalies by seeking smooth models in 3-D. *Geophys. J. Int.* **101,** 157–168.

Scordilis, E. M., (1985). Microseismic study of the Servomacedonian zone and the surrounding area. Ph.D. Thesis, University of Thessaloniki, (in Greek), 250pp.

Spakman, W., and G. Nolet, (1988). Imaging algorithms, accuracy and resolution in delay time tomography. In *Mathematical Geophysics*, ed. N.J. Vlarr, G.Nolet, M.J.R. Wortel and S.A.P.L. Cloetingh, pp. 155–187. Reidel, Dordrecht.

Tarantola, A. and Nercessian, A. (1984) Three-dimensional inversion without blocks. *Geophys. J. R. Astr. Soc.* **79,** 299–306.

Thurber, C. H. (1983) Earthquake locations and three-dimensional crustal structure in the Coyote Lake area, central California. *J. Geophys. Res.* **88,** 8226–8236.